ASSESSMENT OF THE HARMONIC BALANCE METHOD FOR ROTOR BLADE PERFORMANCE PREDICTIONS

Thomas A. Fitzgibbon, Mark A. Woodgate and George N. Barakos
CFD Laboratory, School of Engineering, University of Glasgow, G12 8QQ, U.K.

Abstract

This paper presents an assessment of the harmonic balance method for rotor blade performance predictions. The harmonic balance method within the HMB3 solver of Glasgow University has been extended to the use with overset grids, and results are presented for the PSP and AH-64A rotor blades in hover and forward flight. The predictions are compared with results from steady-state and time marching simulations. In particular, the harmonic balance method is assessed for capturing key flow features, such as the strength of the advancing blade shockwave and retreating side blade dynamic stall. The limitations of the method are also discussed. The findings show that the harmonic balance method is a promising alternative to time-marching simulations due to a significant reduction in computational costs, leading to the potential use of high-fidelity Navier-Stokes methods in optimisation studies.

1 INTRODUCTION

In the past, many computational methods have been used for rotor performance predictions in hover and forward flight. These range from simple analytical methods such as actuator disk theory and blade element momentum theory, to high-fidelity Navier-Stokes solvers. It has been recognised, that to accurately represent that flow physics around a helicopter rotor, high fidelity methods must be used which resolve the rotor tip vortex formation and roll-up processes, the vortex convection and interaction with the next blade. Accuracy is key in flows around advanced rotor blade planform shapes, where the assumptions used by comprehensive rotor codes may no longer be valid. In recent years, fully-resolved Navier-Stokes time-marching simulations are primarily used within the rotorcraft community for high-fidelity performance predictions. However, these types of simulations are associated with high computational costs. Techniques such as adaptive grid refinement (AMR) and the use of higher order solvers have allowed to lower the required grid sizes, leading to improvements in the simulation time (or higher fidelity representation of the flow field). Another solution for reducing computational cost are frequency domain methods, which are investigated within this paper.

In the past, frequency domain methods have primarily been used for predictions of limit cycle oscillations [1, 2, 3] and have gained considerable popularity in the field of turbomachinery [4, 5, 6]. Other applications include dynamic derivative predictions [7] and wind turbine flows [8]. The key assumption of flow periodicity in frequency domain methods make them well suited to many rotorcraft problems. First solutions for flow fields around helicopter rotors started appearing in the late 2000s. Ekici et al. [9] used an inviscid harmonic balance method for the Caradonna-Tung rotor in hover and forward flight. The method used here, utilised steady-state acceleration techniques such as local time stepping and multigrid acceleration. Gopinath and Jameson [10] developed a time-spectral method for the Navier-Stokes equations using a spectral Fourier collocation matrix. The method used explicit treatment of the source term with artificial dissipation and was later applied to rotorcraft flows by Butsuntorn and Jameson [11] for the Caradonna Tung rotor. Choi et al. [12] used the same time-spectral formulation for a wide range of validation studies for the UH-60A rotor blade at three flight conditions. Full rotor simulations were performed along with single-blade coupled with free wake analysis to further reduce computational costs. Further studies by Choi and Datta [13] examined the method for vibratory load predictions. The majority of these methods, however, are explicit in nature. Woodgate and Barakos [14] de-

veloped a fully-implicit harmonic balance method (also used in this work) and applied it to a range of cases including the UH-60A rotor in forward flight. This method was also used by Johnson and Barakos [15] for optimisation of a rotor blade with a BERP-like blade tip using artificial neural networks as a metamodel and genetic algorithms.

As frequency domain methods, reduce the solution to a large steady state problem, these methods are attractive for adjoint optimisation studies. The spectral method used by Choi et al. [16] was coupled with the adjoint method in an optimisation study of the UH-60A rotor blade in hover and moderate loading high speed forward flight conditions. Here, the flow was modeled as inviscid and a single blade approximation was used. An inviscid harmonic balance implementation was also used for turbomachinery optimization [17]. Fully-turbulent harmonic balance adjoint implementations, however, are starting to appear in literature [18].

Research in harmonic balance methods for overset grids has also been a growing subject of research. Mavriplis et al. [19] developed a time-spectral method for periodic and quasi-periodic flows with slow transients and presented results with Chimera grids. Here, the a Poisson equation solver is implemented in the cells which would otherwise be blanked out from the solution to ensure smoothness of the flow variables at each of the solution snapshots. A different approach was used by Leffell et al. [20] use Barycentric rational interpolation to represent the solution in the nodes of the flow field, which require additional information. Im et al. [21] developed a implicit harmonic balance method with explicit treatment of the unsteady source term and later, a mapped Chebyshev pseudo-spectral method [22] for overset mesh topologies. However, the treatment of the cells that switch from blanked cells to computational within the solution was not elaborated on.

In this work we present our implementation of the harmonic balance method for overset grids. A re-assessment of the method following the work of Woodgate and Barakos [14] is given for rotor performance predictions for higher quality Chimera grids. The method is first assessed in hover for the PSP rotor blade [23]. In forward flight, results for the AH-64A rotor blade [24] are presented. The results are compared with predictions from time-marching simulations as well as the steady state formulation in hover.

2 CFD METHOD

The Helicopter Multi-Block (HMB) [25, 26] code is used as the CFD solver for the present work. The Navier-Stokes equations are discretised using a cell-centred finite volume approach on a multi-block grid. The semidiscrete form of the system of ordinary differential equations for the three solution formulations applied within this work are shown in equations 1-3.

$$(1) \qquad \frac{dW}{dt} + R(W) = S \qquad \text{Steady}$$

$$(2) \qquad \frac{dW}{dt} + \frac{dW}{d\tau} + R(W) = 0 \qquad \text{Unsteady}$$

$$(3) \qquad \frac{dW_{hb}}{dt} + \omega D W_{hb} + R_{hb}(W) = 0 \qquad \text{HB}$$

where, W is the vector of conserved variables, R is the residual vector, S is the source term, t is the real time step, τ is the pseudo time step, ω is the reduced frequency, D is the Fourier collocation derivative operator and HB refers to the Harmonic Balance method.

For all methods, to evaluate the convective fluxes, the Osher[27] approximate Riemann solver is used, while the viscous terms are discretised using a second order central differencing spatial discretisation. The Monotone Upstream-centred Schemes for Conservation Laws, which is referred to in the literature as the MUSCL approach and developed by Leer [28], is used to provide high-order accuracy in space. The HMB solver uses the alternative form of the Albada limiter [29] being activated in regions where a large gradients are encountered mainly due to shock waves, avoiding the non-physical spurious oscillations.

In the unsteady method, an implicit dual-time stepping technique [30] is employed to performed the temporal integration, where the solution is marched to steady state in pseudo-time τ. In the steady approach the flow field is solved in a non-inertial reference frame with a source term and mesh velocities that account for the centripetal and Coriolis acceleration terms. The harmonic balance method is described in more detail in the next subsection. For all methods the linearised system of equations is solved using the Generalised Conjugate Gradient method with a Block Incomplete Lower-Upper (BILU) factorisation as a pre-conditioner [31]. To allow an easy sharing of the calculation load for parallel job, a multi-block structured meshes are used. For this study, the fully-turbulent Wilcox's k-ω-SST model from Menter [32] is employed.

2.1 Harmonic Balance Method

The harmonic balance method represents the flow solution and residual vectors as a truncated Fourier series, by assuming a periodicity in time with a frequency, ω. The flow is represented by N_H harmonic balance modes and is split into $N_T = 2N_H + 1$ subintervals, which are coupled using the Fourier collocation derivative operator, D. This leads to a significant reduction in computational costs compared to time-marching simulations, as the flow-field can be solved as a large $(N_T \times N_T)$ steady state problem. This work follows the implementation used by Woodgate and Barakos [14].

By starting from the standard system of ordinary differential equations:

$$(4) \qquad I(t) = V\frac{dW(t)}{dt} + R(t) = 0$$

and representing as a truncated Fourier series, we can write:

$$(5) \qquad W(t) = \sum_{k=-N_H}^{N_H} \hat{W}_k e^{ik\omega t}$$

$$(6) \qquad R(t) = \sum_{k=-N_H}^{N_H} \hat{R}_k e^{ik\omega t}$$

$$(7) \qquad I(t) = \sum_{k=-N_H}^{N_H} \hat{I}_k e^{ik\omega t}$$

Using the orthogonality of the Fourier terms for each wave number k we can write:

$$(8) \qquad \hat{I}_k = i\omega k V \hat{W}_k + \hat{R}_k = 0$$

The system is of $N_T = 2N_H + 1$ equations for N_H harmonics and which can be written as:

$$(9) \qquad \omega A \hat{W} + \hat{R} = 0$$

where matrix A is a N_T x N_T matrix. The system is solved using a pseudo-spectral approach by transforming equation 8 back into the time domain and splitting the solution into N_T discrete subintervals over the period $T = 2\pi/\omega$. By using a transformation matrix E, such that $\hat{W} = EW_{hb}$ and $\hat{R} = ER_{hb}$ we can write:

$$(10) \qquad \begin{aligned} \omega AEW_{hb} + E_{hb} = 0 &= \omega E^{-1}AEW_{hb} \\ + E^{-1}ER_{hb} &= \omega DW_{hb} + R_{hb} \end{aligned}$$

where D = $E^{-1}AE$ and is defined as:

$$(11) \qquad D_{i,j} = \frac{2}{N_T} \sum_{k=1}^{N_H} k \sin(2\pi k(j-1)/N_T)$$

Pseudo-time marching is then applied to the equation 12:

$$(12) \qquad \frac{W_{hb}}{dt} + \omega DW_{hb} + R_{hb} = 0$$

The equation is solved using an implicit method with an implicit treatment of the source term (to increase the attainable CFL number) which is solved as follows:

$$(13) \qquad \omega DW_{hb}^{n+1} = \omega DW_{hb}^n + \omega D(\Delta W_{hb})$$

The full harmonic balance equation then becomes:

$$(14) \qquad \frac{W_{hb}^{n+1} - W_{hb}^n}{\Delta t^*} = -\left[\omega DW_{hb}^{n+1} + R_{hb}(W_{hb}^{n+1})\right]$$

An approximate Jacobian matrix is used within the linear system based on first order discretisation of the residual function is used to improve the conditioning of the system. The system is then solved using a Krylov subspace method with BILU factorisation.

The following implementation is different than other commonly used frequency domain methods. The Non-Linear Frequency Domain method of McMullen et al. [33] solves the flow equations directly in the frequency domain, however, the residual was formulated in the time domain. This led to the requirement of fast Fourier transform and inverse fast Fourier transform operations within the iterative process. The present method follows the approach of Hall [4] where a discrete Fourier transformation matrix is used within the harmonic balance equations (within the pseudo-spectral derivative operator), allowing the solution for the Fourier series coefficients and residual to be obtained directly in the time domain. The time-spectral method of Gopinath and Jameson [10] is similar, with a slightly different implementation of the time-derivative term.

2.2 Harmonic Balance Chimera Implementation

The Overset Grid Method implemented within HMB [34] is used for ease of grid generation and to allow for the relative motion between mesh components in forward flight cases. Typically for time-marching simulations, three types of cells are distinguished in the Chimera fringe, including computational cells where the flow is solved, interpolation cells with interpolated values from a higher Chimera grid level and cells flagged as holes where no solution is obtained. In the harmonic balance formulation, the holes will change dynamically between the solution snapshots, leading to a lack of information about the flow field. Here, to deal with the rotational movement of the rotor blades, an intermediate disk chimera level is included in the grid that rotates with the blades, keeping the cell flagging constant. The pitching and flapping motions are solved by flagging holes that dynamically change between snapshots as a interpolation cell. This will give a valid solution as long as the holes representing the solid body do not move out of the foreground grid in any snapshot of the solution, hence are more constrained by high flapping harmonics rather than pitching. An example of the cell flagging procedure for harmonic balance solutions is shown for a pitching 2D NACA0012 aerofoil ($\alpha = 15° \pm 10°$) in figure 1. Here, the holes are shown in blue and dark-blue, the interpolation cells are shown in yellow, whereas the computational cells are shown in green. The key issue with harmonic balance chimera implementations, is that between each snapshot of the solution, the cells flagged as holes (blue and -dark blue) will be different. Therefore, cells that were previously non-computational (blue) with freestream solution values will become computational (green/red). The solution to this problem is to flag all holes that become computational in any snapshot of the solution as interpolation cells (yellow). This can be seen in figure 1, as the layers of interpolation cells vary with each snapshot of the solution, ensuring that all cells that become computational have a valid solution.

3 NUMERICAL SETUP

3.1 Blade Geometries

The two rotor blade planforms used for this study are shown in figure 2.

The four-bladed PSP rotor has an aspect ratio (R/c) of 12.2, a geometric solidity of 0.1033 and a nominal twist of -14 degrees. The blade planform has been generated using three aerofoils. First, the RC(4)-12 aerofoil was used up to 65% R, then, the RC(4)-10 aerofoil from 70% R to 80% R, finally, the RC(6)-08 aerofoil was used from 85% R to the tip. The aerodynamic characteristics of these aerofoils can be found in [35, 36]. The PSP model rotor has a swept-tapered tip outboard of 95%R.

The AH-64A rotor blade geometry was built based on the information provided for the model scale blade by Berry [37] and the rotor design paper by JanakiRam et al. [24]. The AH-64 rotor blade has a swept tip, a linear blade twist of 9 degrees and an aspect ratio of 13.714. The blade is composed of two aerofoil sections, the HH-02 section up to 0.943R and the NACA64A006 section at the tip of the blade. Information about the aerodynamic characteristics of these aerofoils can be found in [38] and [39] respectively. Uncertainties exist regarding the aerofoil orientation across the swept tip, which was assumed normal to feathering axis. The blade twist was applied about the quarter chord point of each section, not the twist axis, to prevent blade dihedral. The blending between the two aerofoils is another uncertainty as the HH-02 aerofoil has a trim tab, whereas the NACA64A006 section does not. The thickness of the trailing edge for each of the aerofoils is also slightly different, and was matched to the thickness of the HH02 section.

3.2 Computational Setup

The computational meshes for each of the rotor blade geometries were also generated within ICEM-HEXA. For each of the rotor blades, the chimera technique was used, hence a foreground was generated to resolve was generated to resolve the blade geometries, with a background grid to capture the farfield wake geometry. The simulations were performed for isolated rotors, without modeling the fuselage, test stand or facility walls to minimize computational costs. Aeroelastic effects were neglected, as the key of the study is to validate the harmonic balance method in comparison with time-marching simulations. In hover, for the steady state and time-marching simulations a quarter of the computational domain was meshed, assuming periodic conditions for the flow field in the azimuthal direction. A full rotor disk was used for the harmonic balance method. For the steady state simulation a source/sink model is used for the simulations with a Froude boundary condition imposed at the inflow and outflow. The unsteady and harmonic balance solutions used farfield boundary conditions at the domain boundaries. In forward flight, the full rotor disk is modeled for both unsteady and harmonic balance simulations. The hub is modeled as a generic ellipsoidal surface in the time-marching simulations, and it is removed for the harmonic balance solutions to improve the stability of the method [14]. The flow is solved in a cylindrical domain with farfield boundary conditions. The domain used is shown in figure 3 a). For both blades, C-topology around the leading edge of the blade was selected, whereas an H-topology was employed at the trailing edge. A example foreground topology is shown for the AH-64A rotor blade in figure 3 b). The grid sizes for the PSP and AH-64A rotor blades in hover and forward flight are shown in Table 1. Typically 230-260 points are used around the aerofoil with 160-200 points in the spanwise direction. The PSP rotor blade mesh has a wall distance of $1.0 \cdot 10^{-5}$ c_{ref}, whereas the AH-64A mesh has a wall distance of $1.0 \cdot 10^{-6}$ c_{ref} to ensure a $y^+ < 1$.

4 RESULTS AND DISCUSSION

4.1 Hover Flight

In hover, simulations are performed for the PSP rotor blade [23] at $M_{tip} = 0.65$ and 9 degrees collective. The Reynolds number was based on the reference blade chord equal to 5.45 inches and equal to 2.16×10^6. The steady computation was performed for 120,000 iterations, whereas the unsteady simulation was performed for 30 revolutions at 0.5 degree time steps. A one mode harmonic balance computation was performed for 20,000 iterations. The differences in rotor performance predictions and computational resources used are shown in Table 2. The integrated loads for the unsteady and harmonic balance simulations are averaged from one revolution.

The performance results for the steady, unsteady and harmonic balance formulations are in very good agreement. The differences in figure of merit are within 1 count, showing the capability of the harmonic balance method to accurately predict hover performance. The steady state and harmonic balance formulations lead to significant computational cost savings compared to the unsteady simulation. The excellent agreement of the three solutions is confirmed by the surface pressure at r/R = 0.75 and r/R = 0.975, shown in figure 4. The three methods show minor differences in the suction peak predictions at the two examined radial stations.

Further analysis is performed by extracting the wake geometries for each of the methods, shown in figure 5. The flow topologies show similar characteristics, with the main differences being in the root region. The low dynamic head present near the hub in the hover condition, leads to slow transient flow features which are difficult to fully converge. However, as seen by the integrated loads predictions, the flow near the root has a minor impact on the overall rotor performance. The unsteady and harmonic balance simulations were performed with farfield boundary conditions leading to slow

development of the rotor wake in hover, especially near the blade root. Application of Froude boundary conditions could potentially lead to faster development of the wake structure near the blade root leading to improved overall convergence of the flow field and is seen as part of future work.

4.2 Forward Flight

In forward flight, simulations are performed for the full-scale AH-64A rotor blade [24] at $M_{tip} = 0.65$. The Reynolds number was based on the reference blade chord equal to 21 inches and equal to 7.99×10^6. The case chosen for the AH-64 rotor blade in forward flight is at an advance ratio, $\mu = 0.3$ and thrust coefficient, $C_T = 0.00903$. This condition exhibits adverse flow features such as a advancing blade shock and dynamic stall on the retreating side. The time-marching simulation was performed for four revolutions with a 0.5 degree time step. The flow field for this case is shown in figure 6. Due to the highly nonlinear flow phenomena present in this condition, it is considered as a difficult case for the harmonic balance method. Harmonic Balance calculations are performed for a various number of modes: one, four and seven. This is done to show how the solution fidelity increases. All harmonic balance computations were simulated for 15,000 iterations and showed good convergence of the rotor loads. The results from the harmonic balance computations are compared with the time-marching predictions. The trim state for this condition was obtained from a time-marching simulation which used a matrix trimming routine [25] to achieve the target thrust coefficient whilst minimising pitching and rolling moments. The computed trim state is shown in table 3 and is used within the harmonic balance calculations.

Firstly, the rotor disk load distributions are extracted from the solutions shown in figure 7, for a qualitative assessment of the harmonic balance prediction of rotor blade loads. The normal force distributions show good qualitative agreement. Even for one harmonic balance mode, the main lifting areas of the rotor disk are well predicted, with certain differences seen on the advancing and retreating side. With four harmonic balance modes, the agreement improves in these regions. The seven mode calculation when compared to the four mode prediction, improves the agreement at the front of the rotor disk and advancing side, when compared to the time-marching calculation. The pitching moment distributions indicate a clear dynamic stall occurance in the mid span region on the retreating side, due to the strong nose-down pitching moment. With increasing number of modes, the region of dynamic stall is captured in more precise manner. However, based on the results it can be stated that a higher number of modes would be beneficial. The chordwise force distributions are also well captured. The magnitude of the chordwise force is underpredicted on both the retreating side and on the advancing blade when compared to the time-marching calculation, although the agreement improves with increasing number of modes.

The results are compared in a more quantitative manner by extracting the azimuthal loads at three radial stations. The normal force predictions are in very good agreement especially for the cases four mode and seven mode harmonic balance calculations. A certain phase shift can be seen on the advancing and retreating side due to the complex flow physics associated with the formation of the advancing blade shockwave and retreating blade dynamic stall. This can especially be seen in the pitching moment curves as certain non-linearities associated with these features, lead to poor predictions in these regions. A high number of modes is required to resolve these flow features more precisely. The chordwise force predictions are reasonable with a significant underprediction on the retreating side and front of the disk. The overall trends and magnitude, however, are well captured.

A more detailed analysis is performed for the advancing and retreating blades. The surface pressure distribution on the advancing blade is shown in figure 9. The harmonic balance solutions are able to capture this feature with good agreement. The one mode solution does not predict the presence of the shockwave, whereas the four and seven mode harmonic balance solutions are much closer to the time-marching prediction. The four and seven mode harmonic balance solutions lead to a better capturing of the shock location. The seven mode solution, also, has an improved prediction of the blade loading further inboard. This is shown more quantitavely in figure 10, through a chordwise surface pressure distribution at r/R = 0.90 and the radial normal force distribution. The surface pressure distribution shows that the four mode harmonic balance calculation captures the chordwise shock position very accurately, whereas the seven mode solution leads to an improved radial loading on the advancing side.

The retreating side is also analysed in more detail. The surface pressure distributions at 270° azimuth are shown in figure 11. The predictions show that the location, and effect on blade loading of the dynamic stall vortex is difficult to predict using the harmonic balance method. This is a highly nonlinear phenomenon which would require a very high number of modes to capture accurately. However, the seven mode calculation predicts of the reduced blade loading near the trailing edge fairly well. This is also confirmed by the sectional pitching moments shown in figure 12, as the location at which a nose-down pitching moment indicating the presence of dynamic stall is predicted very well for the seven mode harmonic balance case. Another important aspect, is that the loading is underpredicted at the blade tip on the retreating side for all the harmonic balance cases.

Finally, in terms of computational costs, savings up to 40% (dependent on the number of modes) are possible with the current formulation, with more efficiencies currently being investigated.

5 CONCLUSIONS AND FUTURE WORK

The results in this paper show the harmonic balance method is a promising alternative to computationally expensive time-marching simulations. Very good predictions of the rotor loading were obtained in both hover and forward flight at significantly reduced computational costs. However, to accurately capture flow phenomena such as dynamic stall, a high number of modes are required. For rotor design studies, the exact physics of these flow features are of less importance and the relative changes between different designs become significant. This makes the harmonic balance method well suited for optimisation studies as the method maintains the fidelity of Navier-Stokes methods, and can capture the correct loading trends with only a few modes. Future work includes coupling the harmonic balance method with the adjoint method and performing optimisation of a rotor blade in hover and forward flight.

6 Acknowledgments

7 REFERENCES

References

[1] Gopinath, A., Beran, P., and Jameson, A., "Comparative Analysis of Computational Methods for Limit-Cycle Oscialltions," *47th AIAA/ASME/ASCE/AHS/ASC Structures, Structural Dynamics and Materials Conference*, Newport, Rhode Island, 2006.

[2] Thomas, J., Dowell, E., and Hall, K., "Modelling Viscous Transonic Limit-Cycle Oscillation Behavior Using a Harmonic Balance Approach," *Journal of Aircraft*, Vol. 41, No. 6, 2004, pp. 1266–1274.

[3] Yao, W. and Marques, S., "Prediction of Transonic Limit-Cycle Oscillations Using an Aeroelastic Harmonic Balance Method," *AIAA Journal*, Vol. 53, No. 7, 2015, pp. 2040–2051.

[4] Hall, K., Thomas, J., and Clark, W., "Computation of Unsteady Nonlinear Flows in Cascades Using a Harmonic Balance Technique," *AIAA Journal*, Vol. 40, No. 5, 2002, pp. 879–886.

[5] Sicot, F., Gomar, A., Dufour, H., and Dugeai, A., "Time-Domain Harmonic Balance Method for Turbomachinery Aeroelasticity," *AIAA Journal*, Vol. 52, No. 1, 2014, pp. 62–71.

[6] van der Weide, E., Gopinath, A., and Jameson, A., "Turbomachinery Applications with the Time Spectral Method," *35th AIAA Fluid Dynamics Conference and Exhibit*, Toronto, Ontario, 2005.

[7] da Ronch, A., McCracken, A., Badcock, K., Widhalm, M., and Campobasso, M., "Linear Frequency Domain and Harmonic Balance Predictions of Dynamic Derivatives," *Journal of Aircraft*, Vol. 50, No. 3, 2013, pp. 694–707.

[8] Campobasso, M., Drofelnik, J., and Gigante, F., "Comparative Assessment of the Harmonic Balance Navier Stokes Technology for Horizontal and Vertical Axis Wind Turbine Aerodynamics," *Journal of Computers & Fluids*, Vol. 136, No. 10, 2016, pp. 354–370.

[9] Ekici, K., Hall, K., and Dowell, E., "Computationally fast harmonic balance methods for unsteady aerodynamic predictions of helicopter rotors," *Journal of Computational Physics*, Vol. 227, No. 12, 2008, pp. 6206–6225.

[10] Gopinath, A. and Jameson, A., "Time Spectral Method for Periodic Unsteady Computations over Two- and Three- Dimensional Bodies," *43rd AIAA Aerospace Sciences Meeting and Exhibit*, Reno, Nevada, 2005.

[11] Jameson, N. B. A., "Time Spectral Method for Rotorcraft Flow," *46th AIAA Aerospace Sciences Meeting and Exhibit*, Reno, Nevada, 2008.

[12] Choi, S., Alonso, J., van der Weide, E., and Sitaraman, J., "Validation Study of Aerodynamic Analysis Tools for Design Optimization of Helicopter Rotors," *25th AIAA Applied Aerodynamics Conference*, Miami, Florida, 2007.

[13] Choi, S. and Datta, A., "Time-Spectral Method for CFD Prediction of Helicopter Rotor Vibratory Loads," *5th International Conference on CFD*, Seoul, Republic of Korea, 2008.

[14] Woodgate, M. and Barakos, G., "Implicit Computational Fluid Dynamics Methods for Fast Analysis of Rotor Flows," *AIAA Journal*, Vol. 50, No. 6, 2012, pp. 1217–1244.

[15] Johnson, C. and Barakos, G., "Optimizing Rotor Blades with Approximate British Experimental Rotor Programme Tips," *Journal of Aircraft*, Vol. 51, No. 2, 2014, pp. 447–463.

[16] Choi, S., Lee, K., Potsdam, M., and Alonso, J., "Helicopter Rotor Design Using a Time-Spectral and Adjoint-Based Method," *Journal of Aircraft*, Vol. 51, No. 2, 2014, pp. 412–423.

[17] Huang, H. and Ekici, K., "A discrete adjoint harmonic balance method for turbomachinery shape optimization," *Journal of Aerospace Science and Technology*, Vol. 39, 2014, pp. 481–490.

[18] Rubino, A., Pini, M., Colonna, P., Albring, T., Nimmagadda, S., Economon, T., and Alonso, J., "Adjoint-based fluid dynamic design optimization in quasi-periodic unsteady flow problems using a harmonic balance method," *Journal of Computational Physics*, Vol. 372, 2018, pp. 220–235.

[19] Mavriplis, D., Yang, Z., and Mundis, N., "Extensions of Time Spectral Methods for Practical Rotorcraft Problems," *50th AIAA Aerospace Sciences Meeting*, Nashville, Tennesee, 2012.

[20] Leffell, J., Murman, S., and Puliam, T., "Time-Spectral Method for Overlapping Meshes," *AIAA Journal*, Vol. 55, No. 10, 2017, pp. 3381–3398.

[21] Im, D., Choi, S., and Kwon, H., "Unsteady rotor flow analysis using a diagonally implicit harmonic balance method and an overset mesh topology," *International Journal of Computational Fluid Dynamics*, Vol. 29, No. 1, 2015, pp. 82–99.

[22] Im, D. and Choi, S., "Helicopter Rotor Flow Analysis Using Mapped Chebyshev Pseudospectral Method and Overset Mesh Topology," *Journal of Mathematical Problems in Engineering*, Vol. 2018, 2018.

[23] Wong, O., Watkins, A., Goodman, K., Crafton, J., Forlines, A., Goss, L., Gregory, J., and Juliano, T., "Blade Tip Pressure Measurements using Pressure Sensitive Paint," *American Helicopter Society 68th Annual Forum*, 2012.

[24] JanakiRam, R., Smith, R., Charles, B., and Hassan, A., "Aerodynamic Design of a New Affordable Main Rotor for the Apache Helicopter," *American Helicopter Society 59th Annual Forum*, 2003.

[25] Steijl, R., Barakos, G. N., and Badcock, K., "A framework for CFD analysis of helicopter rotors in hover and forward flight," *International Journal for Numerical Methods in Fluids*, Vol. 51, No. 8, 2006, pp. 819–847, DOI: 10.1002/d.1086.

[26] Steijl, R. and Barakos, G. N., "Sliding mesh algorithm for CFD analysis of helicopter rotor-fuselage aerodynamics," *International Journal for Numerical Methods in Fluids*, Vol. 58, No. 5, 2008, pp. 527–549, DOI: 10.1002/d.1757.

[27] Osher, S. and Chakravarthy, S., "Upwind schemes and boundary conditions with applications to Euler equations in general geometries," *Journal of Computational Physics*, Vol. 50, No. 3, 1983, pp. 447–481, DOI: 10.1016/0021-9991(83)90106-7.

[28] van Leer, B., "Towards the ultimate conservative difference scheme. V.A second-order sequel to Godunov's Method," *Journal of Computational Physics*, Vol. 32, No. 1, 1979, pp. 101–136, DOI: 10.1016/0021-9991(79)90145-1.

[29] van Albada, G. D., van Leer, B., and Roberts, W. W., "A Comparative Study of Computational Methods in Cosmic Gas Dynamics," *Astronomy and Astrophysics*, Vol. 108, No. 1, 1982, pp. 76–84.

[30] Jameson, A., "Time-Dependent Calculations Using Multigrid, with Applications to Unsteady Flows past Airfoils and Wings," *AIAA 10th Computational Fluid Dynamics Conference*, 1991.

[31] Axelsson, O., *Iterative Solution Methods*, Cambridge University Press: Cambridge, MA, 1994.

[32] Menter, F. R., "Two-Equation Eddy-Viscosity Turbulence Models for Engineering Applications," *AIAA Journal*, Vol. 32, No. 8, 1994, pp. 1598–1605, DOI: 10.2514/3.12149.

[33] McMullen, M., Jameson, A., and Alonso, J., "Application of a Non-Linear Frequency Domain Solver to the Euler and Navier-Stokes Equations," *40th Aerospac Sciences Meeting & Exhibit*, Reno, NV, 2002.

[34] Jarkowski, M., Woodgate, M., Barakos, G. N., and Rokicki, J., "Towards consistent hybrid overset mesh methods for rotorcraft CFD," *International Journal for Numerical Methods in Fluids*, Vol. 74, No. 8, 2014, pp. 543–576, DOI: 10.1002/fld.3861.

[35] Noonan, K. W., "Aerodynamic Characteristics of Two Rotorcraft Airfoils Designed for Application to the Inboard Region of a Main Rotor Blade," NASA TP-3009, U.S. Army Aviation Systems Command, TR-90-B-005, July 1990.

[36] Noonan, K. W., "Aerodynamic Characteristics of a Rotorcraft Airfoil Designed for the Tip Region fo a Main Rotor Blade," NASA TM-4264, U.S. Army Aviation Systems Command, TR-91-B-003, May 1991.

[37] Berry, J., "Helicopter Blade Dynamic Loads Measured During Performance Testing of Two Scaled Rotors," Tech. rep., National Aeronautics and Space Administration, 1987, NASA-TM-89053.

[38] WJ. McCroskey and KW. McAlister and LW. Carr and SL. Pucci, "An Experimental Study of Dynamic Stall on Advanced Airfoil Sections Volume 1. Summary of the Experiment," Tech. rep., National Aeronautics and Space Administration, 1982, NASA-TM-84245.

[39] Loftin Jr., L., "Theoretical and Experimental Data for a number of NACA 6A-Series airfoil sections," Tech. rep., National Aeronautics and Space Administration, 1948, NASA-TR-903.
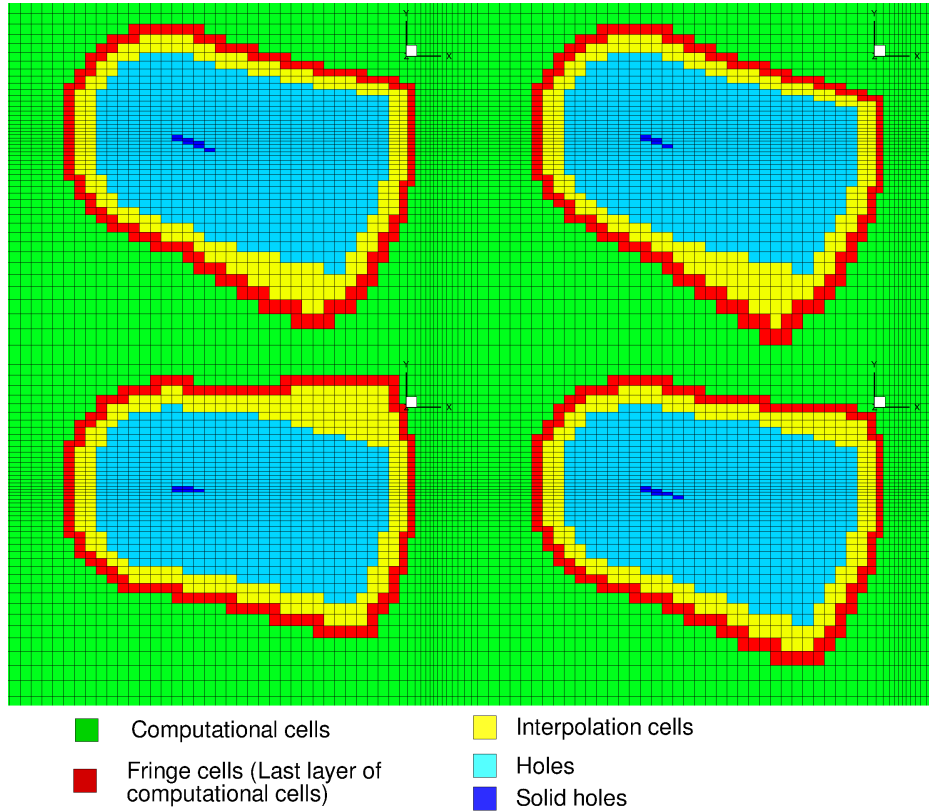
7

8   TABLES AND FIGURES

Figure 1: Example interpolation cell flagging for a pitching 2D NACA0012 aerofoil ($\alpha = 15°\pm10°$). Cell flagging shown for four of the five snapshots of a two mode harmonic balance computation.
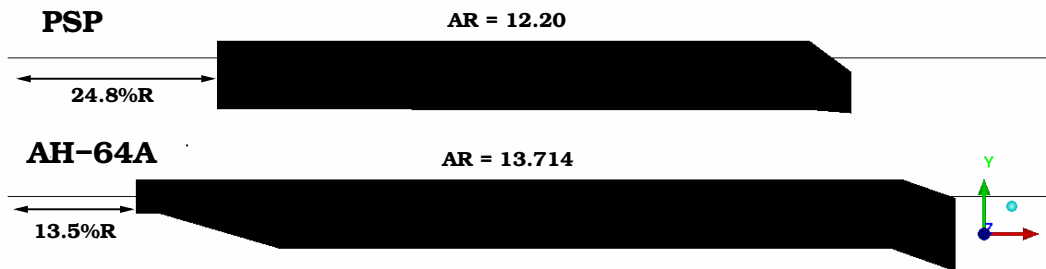

Figure 2: Rotor blade planforms of the PSP [23] and AH-64A [24] rotor blades used for the harmonic balance validation study.

Table 1: Grid sizes in millions of cells for the simulated PSP, Langley Baseline and Langley BERP blades in hover and forward flight.

Solution methodology	Foreground Mesh	Background Mesh	Total mesh size
PSP rotor blade - hover			
Steady	6.3M	7.2M	13.5M
Unsteady	6.3M	7.2M	13.5M
Harmonic Balance	25.2M (4 × 6.3M)	28.8M (4 × 7.2M)	54M
AH-64A rotor blade - forward flight			
All methods	21.6M	11.4M (disk) + 3.1M (background)	36.1M

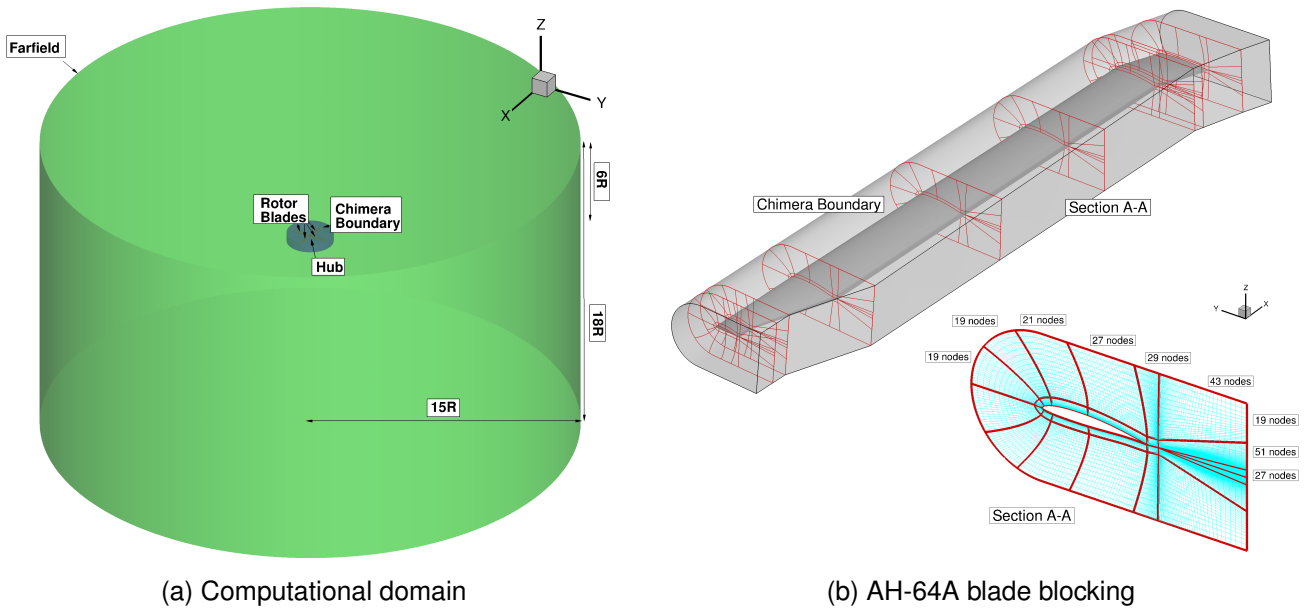(a) Computational domain

(b) AH-64A blade blocking

Figure 3: Computational domain in forward flight and foreground grid blocking for the AH-64A rotor blade.

Table 2: PSP blade hover performance at 9 degrees collective and 0.65 blade tip Mach number using three simulation methods and comparison of computational resources used for each method.

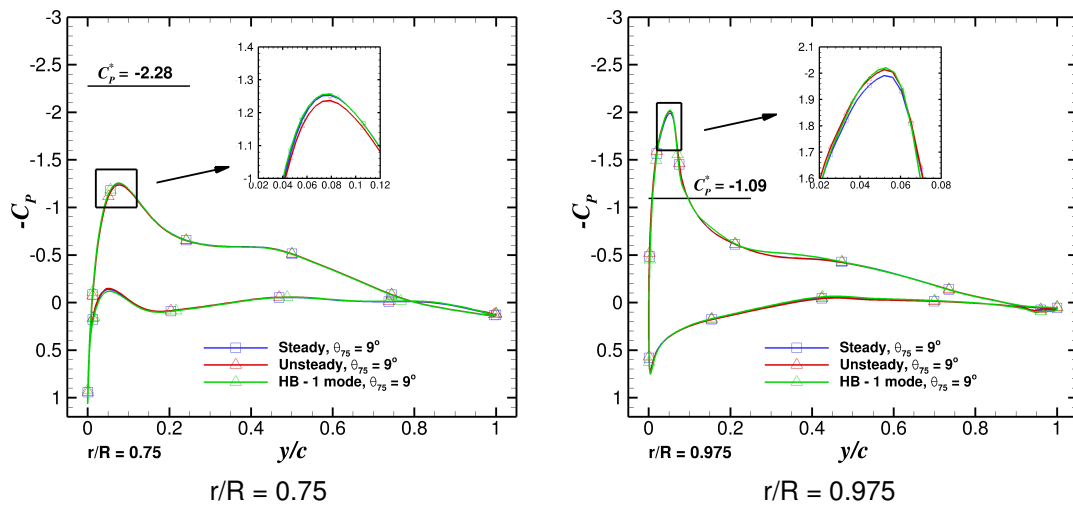| CFD Method	C_T	C_Q	FoM	ΔFoM	CPU time rel. to steady
Steady	0.00759	0.000666	0.702	0.0	1.0
Unsteady	0.00760	0.000665	0.704	+0.2 counts	22.65
Harmonic Balance	0.00754	0.000663	0.698	-0.4 counts	2.02

r/R = 0.75

r/R = 0.975

Figure 4: Comparison of chordwise surface pressure distribution for PSP rotor blade in hover at 9 degrees collective and $M_{TIP} = 0.65$ using three solution methods: steady, unsteady and harmonic balance.
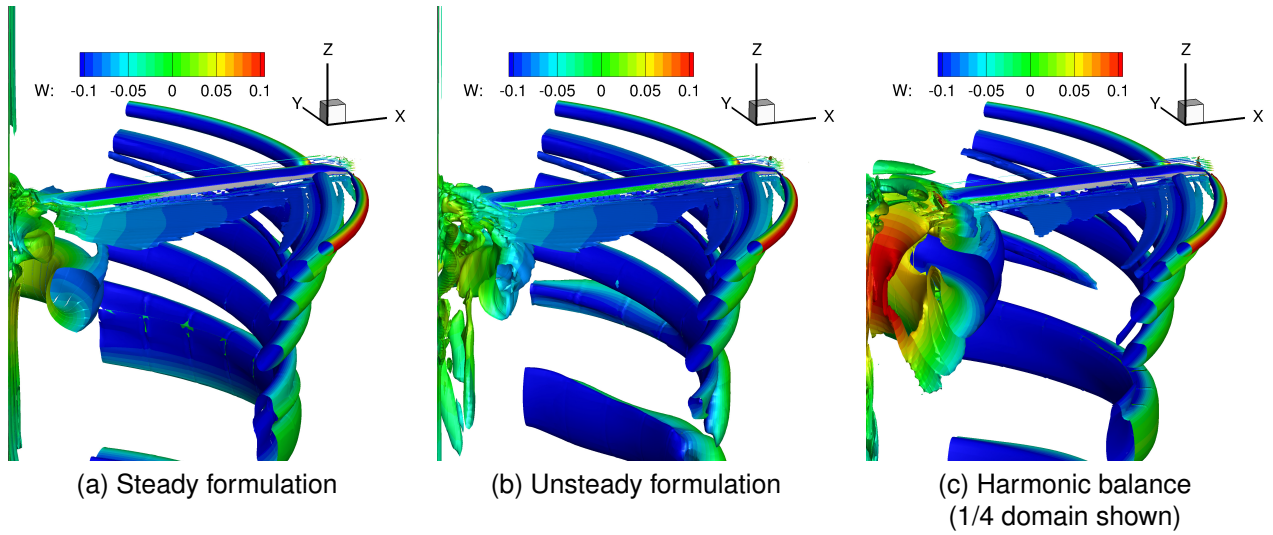
Figure 5: Comparison of wake geometries visualised using Q-criterion (value of 0.0005) coloured with downwash velocity for the PSP blade in hover computed using three CFD formulations.
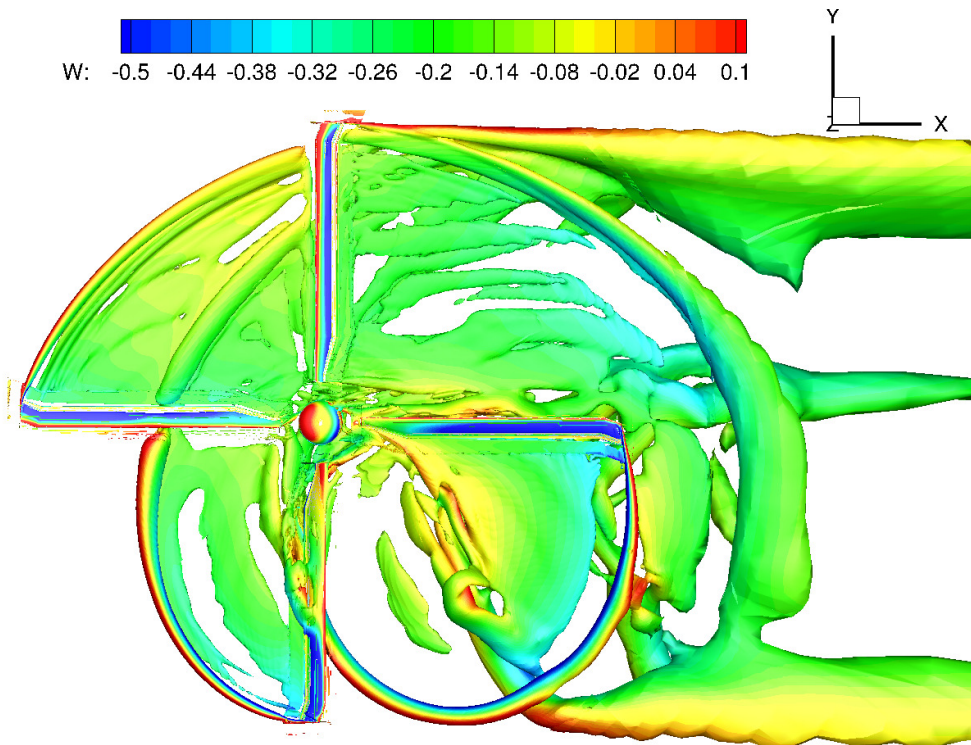

Figure 6: Rotor wake visualization for AH-64A rotor blade in forward flight at $\mu = 0.3$ and $C_T = 0.00903$ using an isosurface of Q-criterion (value of 0.002) coloured by downwash velocity W.

Table 3: AH-64A blade forward flight trim state at $\mu = 0.3$ and $C_T = 0.00903$ used for the simulations within this work. Note: Negative Fourier series used.

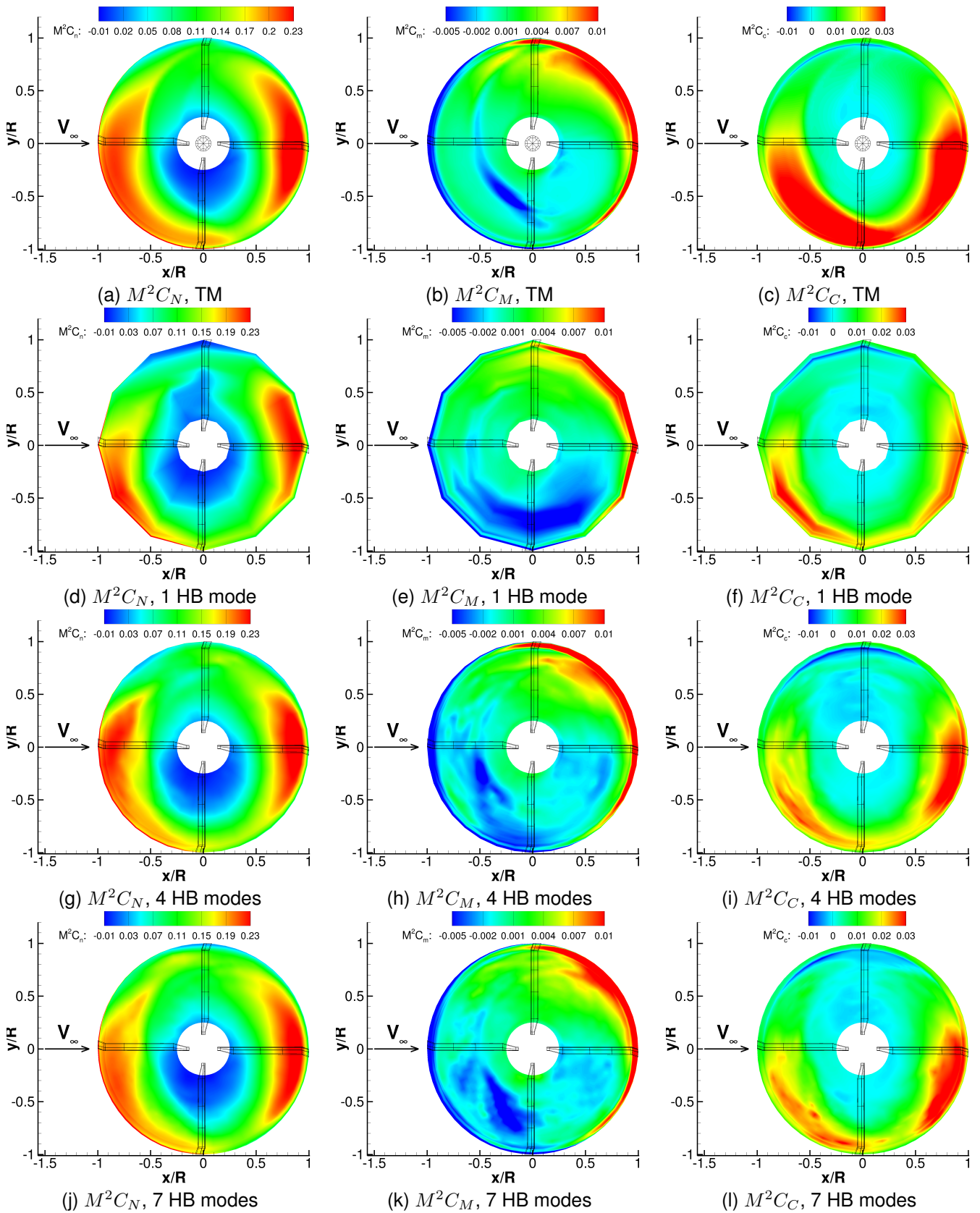| Parameter	Value in degrees
Shaft angle, α_s	-5.431
Collective angle, θ_0	10.413
Lateral cyclic, θ_{1s}	7.421
Longitudinal cyclic, θ_{1c}	-3.072
Coning angle, β_0	3.5
Lateral flapping angle, β_{1s}	0.0
Longitudinal flapping angle, β_{1c}	0.0

10

Figure 7: Rotor disk loads distributions for the AH-64A rotor blade in forward flight at $\mu = 0.3$ and $C_T = 0.00903$ for various number of harmonic balance modes and comparison to time-marching simulation predictions. TM=Time Marching, HB=Harmonic Balance

(a) $r/R = 0.75$, M^2C_N (b) $r/R = 0.9$, M^2C_N (c) $r/R = 0.975$, M^2C_N

(d) $r/R = 0.75$, M^2C_M (e) $r/R = 0.9$, M^2C_M (f) $r/R = 0.975$, M^2C_M

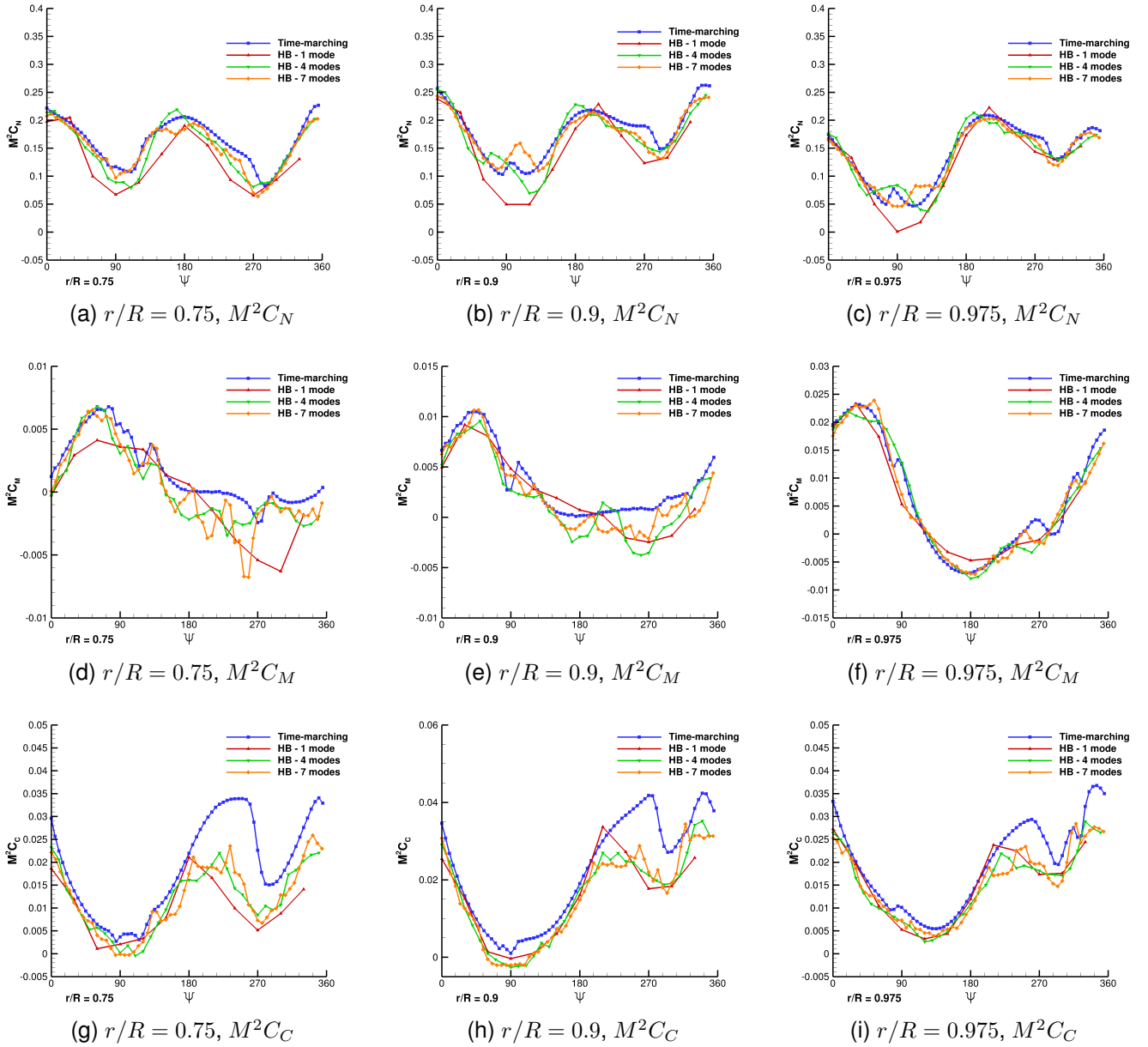(g) $r/R = 0.75$, M^2C_C (h) $r/R = 0.9$, M^2C_C (i) $r/R = 0.975$, M^2C_C

Figure 8: Azimuthal loads at three radial stations for the AH-64A blade in forward flight at $C_T = 0.00903$ and $\mu = 0.3$ for the harmonic balance method with varying number of modes and comparison to time-marching predictions.

(a) Time-marching

(b) 1 Harmonic Balance mode

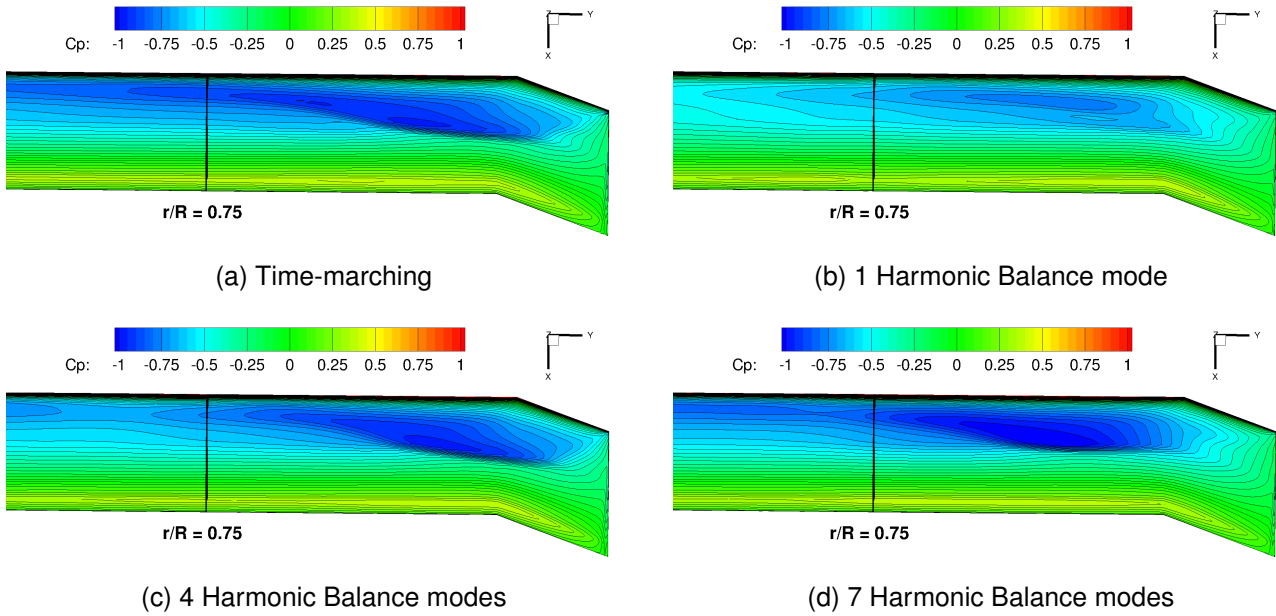(c) 4 Harmonic Balance modes

(d) 7 Harmonic Balance modes

Figure 9: Surface pressure distributions on the advancing side for the AH-64A blade in forward flight at $C_T = 0.00903$ and $\mu = 0.3$ for the harmonic balance method with varying number of modes and comparison to time-marching predictions.
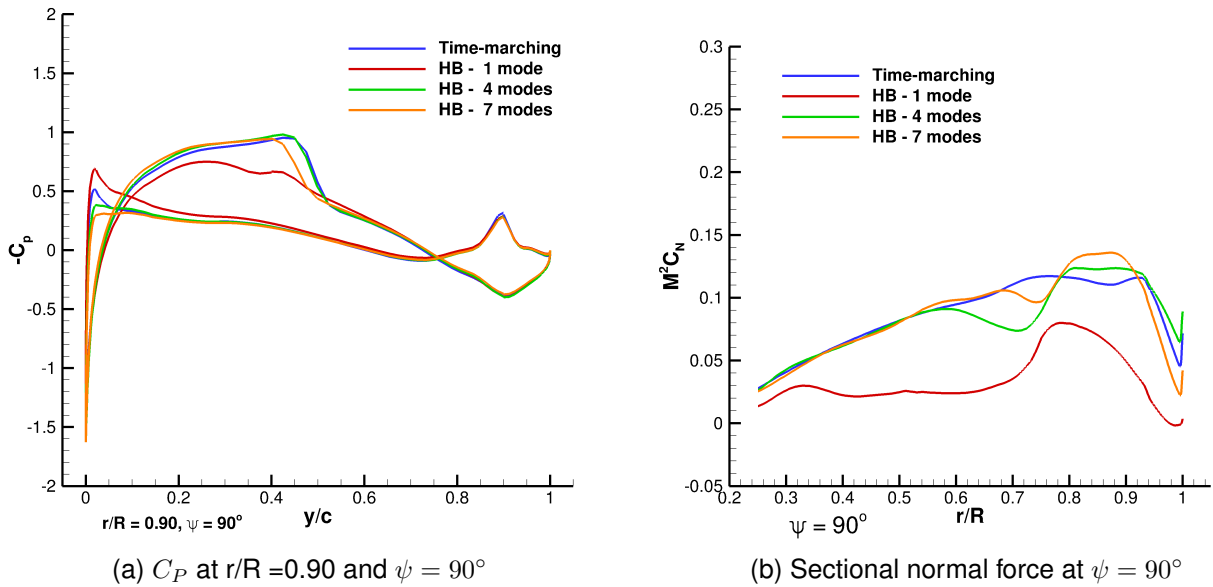

(a) C_P at r/R =0.90 and $\psi = 90°$

(b) Sectional normal force at $\psi = 90°$

Figure 10: Quantitative comparison of the chordwise surface pressure distribution at $\psi = 90°$ and sectional normal force on the advancing side for the AH-64A blade in forward flight at $C_T = 0.00903$ and $\mu = 0.3$ for the harmonic balance method with varying number of modes and comparison to time-marching predictions.

(a) Time-marching

(b) 1 Harmonic Balance mode

(c) 4 Harmonic Balance modes
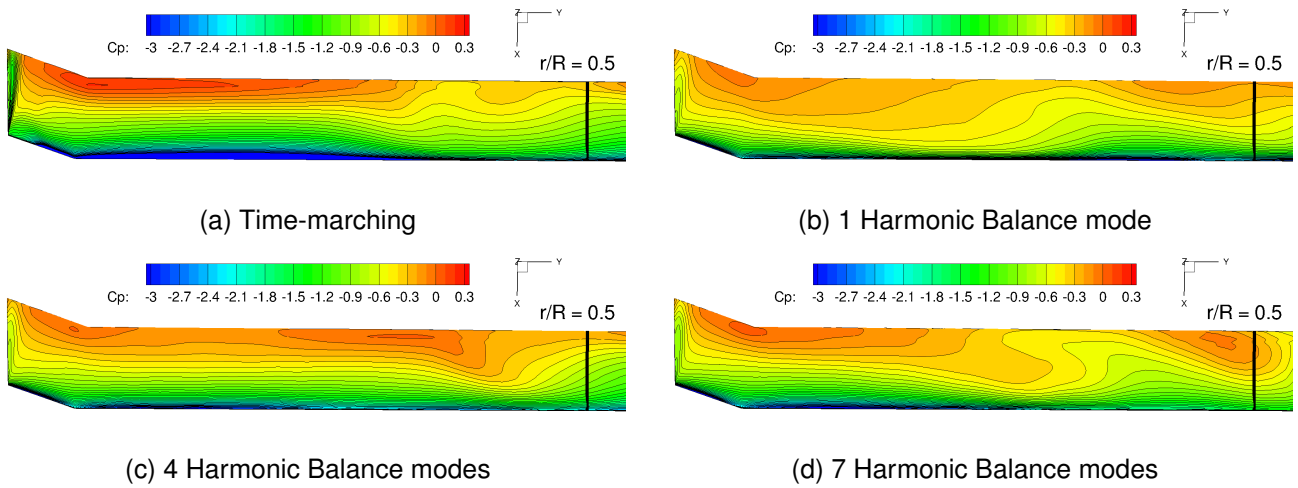
(d) 7 Harmonic Balance modes

Figure 11: Surface pressure distributions on the advancing side for the AH-64A blade in forward flight at $C_T = 0.00903$ and $\mu = 0.3$ for the harmonic balance method with varying number of modes and comparison to time-marching predictions.
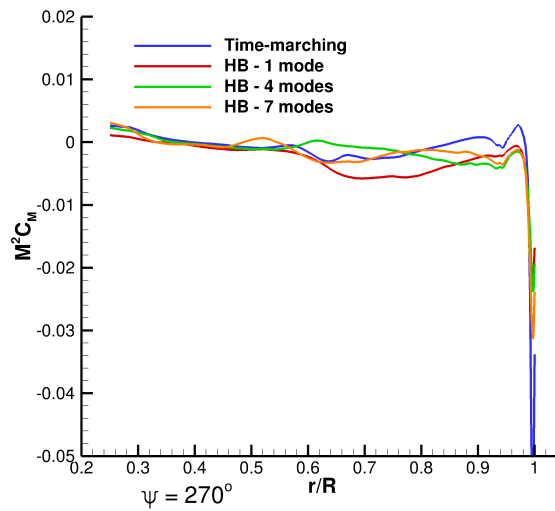

Figure 12: Sectional pitching moment distributions on the retreating side for the AH-64A blade in forward flight at $C_T = 0.00903$ and $\mu = 0.3$ for the harmonic balance method with varying number of modes and comparison to time-marching predictions.

14